



UWL REPOSITORY

repository.uwl.ac.uk

A novel technology for in vivo detection of cell type-specific neural connection with AQP1-encoding rAAV2-retro vector and metal-free MRI

Zheng, Ning, Li, Mei, Wu, Yang, Kaewborisuth, Challika, Li, Zhen, Gui, Zhu, Wu, Jinfeng, Cai, Aoling, Lin, Kangguang, Su, Kuan-Pin, Xiang, Hongbing, Tian, Xuebi, Manyande, Anne ORCID logo ORCID: <https://orcid.org/0000-0002-8257-0722>, Xu, Fuqiang and Wang, Jie (2022) A novel technology for in vivo detection of cell type-specific neural connection with AQP1-encoding rAAV2-retro vector and metal-free MRI. *NeuroImage*, 258. p. 119402. ISSN 1053-8119

<http://dx.doi.org/10.1016/j.neuroimage.2022.119402>

This is the Published Version of the final output.

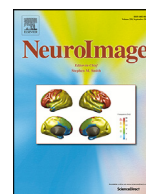
UWL repository link: <https://repository.uwl.ac.uk/id/eprint/9286/>

Alternative formats: If you require this document in an alternative format, please contact: open.research@uwl.ac.uk

Copyright: Creative Commons: Attribution-Noncommercial-No Derivative Works 4.0

Copyright and moral rights for the publications made accessible in the public portal are retained by the authors and/or other copyright owners and it is a condition of accessing publications that users recognise and abide by the legal requirements associated with these rights.

Take down policy: If you believe that this document breaches copyright, please contact us at open.research@uwl.ac.uk providing details, and we will remove access to the work immediately and investigate your claim.



A novel technology for *in vivo* detection of cell type-specific neural connection with AQP1-encoding rAAV2-retro vector and metal-free MRI

Ning Zheng^{a,1}, Mei Li^{b,1}, Yang Wu^{a,c}, Challika Kaewborisuth^d, Zhen Li^e, Zhu Gui^{a,c}, Jinfeng Wu^a, Aoling Cai^a, Kangguang Lin^f, Kuan-Pin Su^g, Hongbing Xiang^e, Xuebi Tian^e, Anne Manyande^h, Fuqiang Xu^{a,b,c,i}, Jie Wang^{a,j,*}

^a Key Laboratory of Magnetic Resonance in Biological Systems, State Key Laboratory of Magnetic Resonance and Atomic and Molecular Physics, National Center for Magnetic Resonance in Wuhan, Innovation Academy for Precision Measurement Science and Technology, Chinese Academy of Sciences-Wuhan National Laboratory for Optoelectronics, Wuhan Institute of Physics and Mathematics, Wuhan 430071, China

^b The Brain Cognition and Brain Disease Institute (BCBDI), NMPA Key Laboratory for Research and Evaluation of Viral Vector Technology in Cell and Gene Therapy Medicinal Products, Shenzhen Key Laboratory of Viral Vectors for Biomedicine, Shenzhen Institute of Advanced Technology, Shenzhen-Hong Kong Institute of Brain Science-Shenzhen Fundamental Research Institutions, Chinese Academy of Sciences, Shenzhen 518055, China

^c University of Chinese Academy of Sciences, Beijing 100049, China

^d Virology and Cell Technology Research Team, National Center for Genetic Engineering and Biotechnology (BIOTEC), National Science and Technology Development Agency (NSTDA), Pathumthani 12120, Thailand

^e Department of Anesthesiology, Tongji Hospital, Tongji Medical College, Huazhong University of Science and Technology, Wuhan, Hubei, China

^f Department of Affective Disorders, The Affiliated Brain Hospital of Guangzhou Medical University, Guangzhou, China

^g Department of Psychiatry, China Medical University Hospital, Taichung City, Taiwan, China

^h School of Human and Social Sciences, University of West London, Middlesex, TW8 9GA, UK

ⁱ Center for Excellence in Brain Science and Intelligence Technology, Chinese Academy of Sciences, Shanghai 200031, China

^j Institute of Neuroscience and Brain Diseases, Xiangyang Central Hospital, Affiliated Hospital of Hubei University of Arts and Science, Xiangyang, Hubei, China

ARTICLE INFO

Keywords:

AQP1
rAAV2-retro vector
Metal-free MRI
Neural connection
Cell type-specific network
In vivo imaging

ABSTRACT

A mammalian brain contains numerous neurons with distinct cell types for complex neural circuits. Virus-based circuit tracing tools are powerful in tracking the interaction among the different brain regions. However, detecting brain-wide neural networks *in vivo* remains challenging since most viral tracing systems rely on postmortem optical imaging. We developed a novel approach that enables *in vivo* detection of brain-wide neural connections based on metal-free magnetic resonance imaging (MRI). The recombinant adeno-associated virus (rAAV) with retrograde ability, the rAAV2-retro, encoding the human water channel aquaporin 1 (AQP1) MRI reporter gene was generated to label neural connections. The mouse was micro-injected with the virus at the Caudate Putamen (CPU) region and subjected to detection with Diffusion-weighted MRI (DWI). The prominent structure of the CPU-connected network was clearly defined. In combination with a Cre-loxP system, rAAV2-retro expressing Cre-dependent AQP1 provides a CPU-connected network of specific type neurons. Here, we established a sensitive, metal-free MRI-based strategy for *in vivo* detection of cell type-specific neural connections in the whole brain, which could visualize the dynamic changes of neural networks in rodents and potentially in non-human primates.

1. Introduction

The mammalian brain contains billions of neurons and numerous other cell types, creating complicated neural networks for cell-cell communication through trillions of synapses (Huang, 2014; Luo et al., 2008, 2018). The complexity of neural networks is vital for processing information in the brain and guiding behavior. Therefore, the elucidation and

visualization of neural connections is essential for examining brain functions and disorders (Hoehn and Aswendt, 2013; Park and Friston, 2013; Roselli and Caroni, 2012; Rubinov and Bullmore, 2013).

The neurotropic virus-based neural circuit tracing tool is a fascinating technology for visualizing neural connectivity. It mediates the stable expression of the transgenes and reporter genes in various types of neurons (Nassi et al., 2015). Through genetic modification, the virus can

* Corresponding author at: Key Laboratory of Magnetic Resonance in Biological Systems, State Key Laboratory of Magnetic Resonance and Atomic and Molecular Physics, National Center for Magnetic Resonance in Wuhan, Innovation Academy for Precision Measurement Science and Technology, Chinese Academy of Sciences-Wuhan National Laboratory for Optoelectronics, Wuhan Institute of Physics and Mathematics, Wuhan 430071, China.

E-mail address: jie.wang@wipm.ac.cn (J. Wang).

¹ These authors contributed equally to this work.

target neurons of a defined cell type, allowing exquisite dissection of cell type-specific neural connections. Such technology has significantly enhanced our knowledge and understanding of the relation between different brain regions (Callaway, 2008; Davidson and Breakefield, 2003; Enquist, 2003; Nassi et al., 2015; Ugolini, 2010). Most viral tracers label the neural networks with fluorescent reporter proteins and require postmortem optical imaging to visualize tracing results. To this end, the fluorescence-based-viral tracer has been limited in its ability to conquer the *in vivo* detection of neural networks due to the ineffective light penetration into deep tissues of living animals. Few methods exist for an *in vivo* dissection of the neural network architecture, especially for cell type-specific neural networks.

In contrast to the optical imaging method, MRI techniques empower the acquisition of images *in vivo* with excellent depth penetration and sufficient spatiotemporal resolution (Dumoulin et al., 2018; Pfister et al., 2012; Shenton et al., 2001). Among MRI-based methods, Manganese-Enhanced MRI (MEMRI) and Diffusion Tensor Imaging (DTI) are effective approaches facilitating the detection of structural connectivity of the whole brain in pre-clinical and clinical researches (Donahue et al., 2016; Le Bihan, 2003; Lin et al., 2014; Mori and van Zijl, 2002; Mori and Zhang, 2006; Pautler et al., 1998; Saar and Koretsky, 2019; Yi-Jen Lin, 1997). Nevertheless, neither of these two methods can feature the neurons and fibers' microstructure nor trace the cell type-specific neural connectivity.

The MRI reporter genes encoding proteins with unique properties to modulate the MRI contrast have been defined and applied to *in vivo* visualization (Farhadi et al., 2021; Gilad et al., 2007, 2008; Mukherjee et al., 2017). Ferritin is one of the metalloproteins classified in the iron-based MRI reporters that can enrich the paramagnetic metal ions, enhance nuclear relaxation rates, and produce T1 or T2 weighted MRI contrast (Cohen et al., 2005; Genove et al., 2005; Iordanova and Ahrens, 2012; Matsumoto and Jasanoff, 2013; Zheng et al., 2019). Previously, we have demonstrated a viral tracer using a neurotropic virus encoding ferritin that can practically achieve MRI-based observation of neural connections in living animals (Cai et al., 2021). Nonetheless, the length of time between the virus injection and the MRI visualization of the neuronal connectivity needs to be improved.

Aquaporin (AQP1), a water channel protein, has been recently reported to be a non-metallic MRI reporter gene (Mukherjee et al., 2016). In this regard, AQP1 increases the Apparent Diffusion Coefficient (ADC) values by altering the tissues' water diffusivity, which corresponds to the darkened intensity presented in the diffusion-weighted magnetic resonance imaging (DWI-MRI). Overexpression of the AQP1 protein produces strong DWI contrast in cells and xenograft tumors (Mukherjee et al., 2016). Compared to the commonly used metalloproteins- and Chemical Exchange Saturation Transfer-based reporters, the AQP1 has lower cytotoxicity and higher sensitivity (Mukherjee et al., 2017).

The rAAV vector, a safe transgene vector for research and gene therapy, has been extensively used as a vehicle for gene transfer in neuroscience researches, helping to understand both the structure and function of neural networks (Betley and Sternson, 2011; Chan et al., 2017; Tenenbaum et al., 2004). In 2016, a new artificial AAV serotype, AAV2-retro, was identified via the directed evolution of AAV (Teruo et al., 2016). The rAAV2-retro vector enters neurons from the nerve terminals and retrograde transports to the axon, reaching the nucleus for gene transduction. Therefore, the rAAV2-retro vector carrying a reporter gene could be utilized for retrograde labeling of neuronal networks projecting to specific brain regions (Zheng et al., 2020).

Additionally, combined with a Cre/loxP-mediated recombination strategy, the insertion of the Cre-dependent gene of interest in the rAAV genome is advantageous for promoting a transgene expression in the specific neuronal cell type (McLellan et al., 2017; Van Duyn, 2001). In combination with the double-floxed inverse orientation (DIO) element and transgenic mouse line expressing Cre recombinase in specific cell type neurons, the rAAV helps to identify and examine the roles

of distinct and specific neuron types in circuit structures and functions (García-Otín, 2006; Luo et al., 2008, 2018).

Herein, we established the rAAV2-retro encoding AQP1 for injecting into the caudate putamen (CPU) region of a mouse brain. Three weeks after the injection, the DWI-MRI was applied to evaluate the CPU-connected networks *in vivo*. Fluorescence imaging was used to verify the MRI tracing results. In addition, the rAAV2-retro bearing Cre-dependent AQP1 gene was used to dissect the CPU-connected network in a specific cell type *in vivo*. Our study offers a promising strategy to longitudinally detect neural connections of the whole brain in a live animal. It is beneficial for exploring the dynamic changes in neural networks under physiological and pathological conditions.

2. Materials and methods

2.1. Animals

All surgical and experimental operations were conducted following the guidelines of the Animal Care and Use Committee of Innovation Academy for Precision Measurement Science and Technology, Chinese Academy of Sciences (Approval number: APM21021A). The adult male C57BL/6 J mice were obtained from the Hunan SJA Laboratory Animal Company (Hunan, China). The Thy1-Cre mice were kind gifts from Professor Shumin Duan (Zhejiang University, Zhejiang, China). All animals were housed under a 12 h light/dark cycle at constant temperature and moisture. The animals were allowed food and water *ad libitum*.

2.2. Experimental setup and plasmid constructions

Four experimental groups were designed to achieve the *in vivo* detection of cell type-specific neuronal connections in the rodent brain (Table 1). The plasmids carrying the EGFP and/or human AQP1 genes used to generate the recombinant AAV vectors (rAAVs) in each experiment were constructed as shown in Table 1. The pAAV-CAG-EGFP-WPRE-polyA (P1: pAAV-EGFP) and pAAV-CAG-DIO-EGFP-WPRE-polyA (P4: pAAV-DIO-EGFP) plasmids were obtained from Brain Case (Brain Case, Shenzhen, China). The human AQP1 gene (GenBank: NM_198,098.1) was synthesized (Shengong, China) and inserted into the pAAV-CAG-EGFP-WPRE-polyA in place of the EGFP to generate the pAAV-CAG-AQP1-WPRE-polyA (P2: pAAV-AQP1). To construct the AQP1 and EGFP co-translational proteins, the 2A self-cleavage sequence (Zheng et al., 2019) was inserted between the two genes. The constructed AQP1-2A-EGFP gene cassette was inserted into the P1 and P4 in place of EGFPs to generate the pAAV-CAG-AQP1-2A-EGFP-WPRE-polyA (P3: pAAV-AQP1-EGFP) and the pAAV-CAG-DIO-AQP1-2A-EGFP-WPRE-polyA (P5: pAAV-DIO-AQP1-EGFP), respectively.

2.3. Production of the rAAVs

The rAAVs were produced in human embryonic kidneys 293 (HEK293, ATCC) cells using a traditional triple-plasmid transfection method (Wu et al., 2018). Briefly, the HEK293 cells at 80% confluence were co-transfected with pAAV-Rep-Cap, pAAV-helper and transfer vectors carrying the gene of interest, using PEI transfection reagent (Polysciences, USA). At 72 h post-infection, cells were harvested and subjected to virus purification. The rAAVs were purified by an iodixanol step density gradient centrifugation (Wu et al., 2021). The purified rAAV titers were determined by qPCR using SYBR GreenER™ PCR Master Mix (Bio-Rad, USA) and specific primers, WPRE: 5'-TCCCATAGTAACGCCAATAGG-3' and R5'-CTTGGCATATGATACACTTGATG-3'. The standard curves were generated by performing 10-fold serial dilutions of the standard plasmids for virus titer calculation.

Table 1
Experimental groups, plasmids, and AAVs used in the study.

Experiments	Plasmid information	Plasmidname	AAV types	rAAVname
<i>In vitro</i> cell culture	P1: pAAV-CAG-EGFP-WPRE-pA P2: pAAV-CAG-AQP1-WPRE-pA P3: pAAV-CAG-AQP1-2A-EGFP-WPRE-pA	pAAV-EGFP pAAV-AQP1 pAAV-AQP1-EGFP		
<i>In vivo</i> expression at a local site	P1: pAAV-CAG-EGFP-WPRE-pA P3: pAAV-CAG-AQP1-2A-EGFP-WPRE-pA		rAAV2/9	rAAV-EGFP rAAV-AQP1-EGFP
<i>In vivo</i> neural connection for a local site	P1: pAAV-CAG-EGFP-WPRE-pA P3: pAAV-CAG-AQP1-2A-EGFP-WPRE-pA		rAAV2-retro	rAAV-retro-EGFP rAAV-retro-AQP1-EGFP
<i>In vivo</i> cell-type-specific neural connection for a local site	P4: pAAV-CAG-DIO-EGFP-WPRE-pA P5: pAAV-CAG-DIO-AQP1-2A-EGFP-WPRE-pA	pAAV-DIO-EGFP pAAV-DIO-AQP1-EGFP	rAAV2-retro	rAAV-retro-DIO-EGFP rAAV-retro-DIO-AQP1-EGFP

2.4. *In vitro* DWI: diffusion-weighted MRI of cell pellets

Baby hamster Syrian kidney cells (BHK21, ATCC) were seeded into 12-well plates for 24 h to reach 80% cell confluence. The BHK21 cells at 80% cell confluence were transfected with 1 μ g of the plasmids (P1, P2, or P3) in 100 μ l of Opti-MEM containing 4 μ l Lipofect2000 DNA Transfection Reagent (Thermo Fisher Scientific, USA). Cells were incubated at 37 °C in 5% CO₂ atmosphere for 48 h. To prepare cell pellets for the *in vitro* MRI, cells were trypsinized, suspended in 100 μ l PBS and gently centrifuged at 350 g for 5 min in 0.2 ml PCR tubes (Mukherjee et al., 2016). The cell pellets were then subjected to the MRI experiments as described below.

All MRI images were acquired in a horizontal bore 7.0 T BioSpec machine (Bruker, Germany). A surface coil with a diameter of 20 mm was used in combination with a birdcage transmit coil. To prevent the nonspecific changes in ADC arising from the temperature, the *in vitro* MRI experiments were conducted under constant temperature (~23 °C) conditions. For the DWI-MRI experiments of cell pellets, a stimulated echo based spin-echo DWI sequence was set-up with the following parameters: TR (repetition time) = 2 s, TE (echo time) = 24.7 ms, δ (diffusion gradient duration) = 7 ms, Δ (diffusion gradient interval) = 400 ms, b values = 100, 300, 500, 800, 1000 s·mm⁻², FOV (field of view) = 3.5 \times 3.5 cm², Matrix size = 256 \times 256, Slice thickness = 2.5 mm. The scanning time was 2 h 16 min in total.

2.5. Stereotaxic surgery

Eight-week-old male mice were anesthetized with pentobarbital sodium (50 mg/kg, *i.p.*), and positioned in a stereotaxic frame (RWD, China). The mouse's skull was exposed and drilled to allow access to a glass micropipette (World Precision Instruments, USA). One microliter of the purified rAAV solution (5 \times 10¹² viral genomes/ml in PBS) was stereotaxically injected into the target region (CPU or Ventral tegmental area (VTA)) based on the stereotaxic coordinates of the mouse brain atlas (Paxinos and Franklin). All types of rAAV were collected as shown in Table 1. The coordinates of the CPU and VTA were provided as following: CPU: 0.51 mm anterior to Bregma, 2 mm lateral from midline, 3.3 mm depth relative to Bregma, VTA: 3.2 mm posterior to Bregma, 0.5 mm lateral from midline, 4.35 mm depth relative to Bregma. The infusion rate was 50 nl/min. After the injection, the pipette was kept in place for 20 min and then slowly withdrawn. The head skin was carefully treated with lidocaine lincomycin gel (Xinya, China) after surgery. When the mice were recovered from anesthesia on a warm pad, they were returned to the home cages.

2.6. *In vivo* DWI

Three weeks after the virus injection, the mice were subjected to the *in vivo* MRI experiments. The mice were anesthetized with 3.5–4.0% isoflurane (RWD, China) and maintained with 1.0–1.5% isoflurane. The breathing rate was monitored and maintained at around 60 breaths/min. A warm water pad was used to stabilize the mice body temperature (~36.5 °C). The mouse brain was scanned using a surface coil (Diameter: 20 mm), and a birdcage transmit coil. For the DWI-MRI experiments, a stimulated echo based spin-echo DWI sequence was utilized with the following parameters: TR = 3 s, TE = 24 ms, δ = 7 ms, Δ = 100 ms, b value = 1000 s·mm⁻², FOV = 1.8 \times 1.8 cm², matrix size = 100 \times 100, slice thickness = 0.8 mm, slice number = 12. The scanning time was 51 min 12 s in total.

2.7. Slice preparation, immunohistochemistry and fluorescence imaging

After MRI scanning, the mice were anesthetized with an overdose of pentobarbital sodium (70 mg/kg) followed by cardiac perfusion using PBS and 4% paraformaldehyde (PFA) solution. The brains were removed and fixed in 4% PFA for 12 h. After fixation, the brains were dehydrated in 30% (w/v) sucrose for 24 h and sectioned into 40 μ m slices with a freezing microtome (Leica, German). The immunohistochemistry staining was performed to visualize AQP1 expression using fluorescence imaging. Briefly, the brain slices were washed with PBS three times (five minutes per wash) and blocked with a blocking solution (10% normal goat serum and 0.3% Triton X-100 in PBS) for 1 h. The slices were then incubated with a rabbit anti-AQP1 antibody (ab219055, Abcam) overnight at 4 °C. After antibody incubation, the slices were washed with PBS three times (five minutes per wash), followed by incubation with a Cy3-conjugated goat anti-rabbit secondary antibody for 2 h at 37 °C in the dark. Nuclei were stained utilizing DAPI (Beyotime, China). The brain slices were imaged with the VS120 virtual microscopy slide scanning system (Olympus, Japan).

2.8. Data analysis

The raw DWI-MRI data was converted to nifti (hdr/img) format using the Bruker2Analyze Converter. The brains were manually extracted using MRICron software (<https://www.nitrc.org/projects/mricron/>). The ADC map was calculated in MATLAB (MathWorks, Inc., USA) from the slope of the logarithmic decay in MRI signal intensity versus b -value. To compare ADC values between groups, the DWI images without the diffusion gradient (b_0 images) were utilized to make a brain template using ANTs (Advanced Normalization Tools, <http://stnava.github.io/ANTs/>).

The b0 images were normalized to the homemade template using the antsRegistrationSyN.sh command in ANTs. The 3D volume image of each mouse was registered to a 3D template. Specifically, the rigid-body, affine and nonlinear transformation were sequentially utilized to align images across different mice. Then the transform information was applied to the ADC maps. The aligned ADC maps in the two groups were compared using the 3dtest++ function in AFNI (<https://afni.nimh.nih.gov/>). The FDR (false discovery rate) values were automatically generated with the 3dtest++, and the results of the 3dtest++ were visualized as overlay by the AFNI GUI and the threshold (FDR q value) was set to 0.05 through the GUI. The *t* value map was then overlapped on the homemade template. To quantitatively measure the ADC difference of the brain regions in the two groups, one standard mouse brain template TMBTA (www.nitrc.org/projects/tmbta_2019), was transformed to our homemade template. The transform information was applied to the eleven ROIs (CSF, SC, CPU_right(R), BLA_R, BLA_left(L), Ctx_R, Ctx_L, Ins_R, Ins_L, Hip_R, Tha_R) as defined in the TMBTA atlas. The average ADC values of the ROIs were obtained and then compared with a two-tailed student *t*-test. Results are presented as Average \pm Standard error (Ave \pm SEM).

3. Data and code availability

The data that support the findings of this study will be made available through a public repository (e.g. OSF repository) upon publication of this paper. The analysis code is openly available on GitHub (https://github.com/zhengningapm/retro_aqp1).

4. Results

4.1. AQP1-encoding rAAV vector causes DWI contrast changes in vitro and in vivo

To examine whether the AQP1-encoding rAAV vector can infect cells and function as a DWI reporter, we first conducted the *in vitro* study in the BHK21 cells. The cells were transfected with each rAAV transfer plasmid (P1, P2, or P3) (Fig. 1A) and collected for MRI scanning. The MRI results showed that DWI signal intensities in the cells expressing either AQP1-EGFP or AQP1 decreased compared to those expressing EGFP alone or the mock control (Sham) (Fig. 1B). Consistently, the ADC of AQP1-expressing cells significantly increased compared to the control cells (Fig. 1C–D), suggesting that the rAAV vectors encoding the AQP1 could be used as a DWI reporter.

We next investigated whether the rAAV encoding AQP1 could be visualized by the *in vivo* DWI. The rAAV-AQP1-EGFP or rAAV-EGFP that allow local expression of the exogenous gene at the initial infection site were stereotactically injected into the bilateral CPU regions in the mouse brain (Fig. 2A, *n* = 4). After 21 days' infection, the living mouse brain was imaged using the MRI scanner. The brain region injected with the rAAV-AQP1-EGFP represented a strong DWI contrast and higher ADC value than those at the contralateral region (Fig. 2A, B). The expression of AQP1-EGFP and EGFP in the bilateral CPU regions was confirmed by immunohistochemistry staining and fluorescent imaging of brain slices (Fig. 2C). The haematoxylin-eosin staining result revealed that there was no edema or necrosis in either the AQP1-EGFP or EGFP expressing brain regions (Fig. S1), which is consistent with findings of a previous report (Mukherjee et al., 2016).

To examine the effect of AQP1-encoding rAAV on the neuronal functions, the patch experiments were conducted in mice infected with the rAAV-AQP1-EGFP and rAAV-EGFP in bilateral CPU regions. The results showed no significant difference in the fundamental electrical characteristics between the neurons infected with the rAAV-AQP1-EGFP and rAAV-EGFP (Fig. S2).

4.2. Detection of the neural connections using in vivo DWI

To detect the neural connection of the whole brain in living animals, the retrograde AAV vectors (rAAV2-retro) were utilized to trace the upstream brain regions of the injected site. Five mice were included in each group. The rAAV2-retro expressing AQP1-EGFP (rAAV-retro-AQP1-EGFP) or EGFP alone (rAAV-retro-EGFP) were constructed and micro-injected into the CPU region. 21 days after infection, the living mouse brain was imaged using the *in vivo* DWI method. The patterns of the GFP signals in both groups were similar, suggesting that the different rAAV2-retro vectors retrograde to the same brain regions (Fig. 3). No discernable hypointensity MRI contrast was observed in the brain infected with rAAV-retro-EGFP (Fig. 4A). However, the DWI images of the rAAV-retro-AQP1-EGFP group exhibited a significant change in intensity (Fig. 4B). Hypointensity DWI contrast could be found in multiple brain regions, including the injection site of the right CPU, Ctx (cerebral cortex), BLA (basolateral amygdala), Ins (insular cortex), right Tha (thalamus), right HIP (hippocampus). The ADC map of all mice in the rAAV-retro-AQP1-EGFP and the rAAV-retro-EGFP groups were calculated and compared. The ADC values of several regions in the rAAV-retro-AQP1-EGFP group were higher than the rAAV-retro-EGFP group (Fig. 4C) and overlapped with the regions that showed hypointensity DWI signals (Fig. 4B). The presence of AQP1 expression in brain regions of the rAAV-retro-AQP1-EGFP group was observed using immunohistochemistry staining (Fig. 4D). To illustrate the correlation between the results of MRI and immunohistochemistry in the structural brain regions or sub-regions, the mouse brain atlas (Paxinos and Franklin) was superimposed with the images (Fig. S3). Although the resolution of the DWI-MRI was much lower than the fluorescence imaging, the AQP1 expression and AQP1-based MRI contrasts could be detected in the same locations. Extensive overlap areas of the DWI-MRI contrast and AQP1 expression signals (Figs. 4B–D and S3) were also found, suggesting pronounced activity of the AQP1 as a DWI-MRI reporter. These tracing results are consistent with the reported anatomical connectivity of the CPU (Davidsson et al., 2019; Tervo et al., 2016).

To further validate the MRI-based *in vivo* neural connections tracing method, the rAAV2-retro-AQP1-EGFP was injected into the VTA region that receives abundant input from the cerebral cortex. As found in the CPU region (Fig. 4), the neural connections of VTA were also successfully visualized by both MRI and fluorescence imaging approaches (Fig. S4).

To this end, we have successfully established the rAAV2-retro-AQP1-EGFP that is able to effectively express the AQP1 and trace the neural connections visualized by both the *in vivo* DWI and fluorescent imaging.

4.3. Quantification of ADC values in the AQP1 transduction regions

To quantify the alteration of DWI contrast, the ADC values of the rAAV-retro-AQP1-EGFP and the rAAV-retro-EGFP groups were calculated and compared. The mean ADC values of AQP1 transduction brain regions, including the caudate putamen (CPU), basolateral amygdala (BLA), cerebral cortex (Ctx), insular cortex (Ins), thalamus (Tha), hippocampus (Hip), were measured and collected (Figs. 4D and 5A). The superior colliculus (SC) region was selected as the negative control since neither the green fluorescent signal nor the hypointensity DWI contrast was observed in this region. The ADC values of the cerebrospinal fluid (CSF) were also used as the negative control. Increased ADC values of the AQP1 transduction regions were detected in the rAAV-retro-AQP1-EGFP group (Fig. 5B). These results indicate that the CPU-connected upstream connections were specified using a combination of the rAAV-retro-AQP1-EGFP vector and the *in vivo* DWI.

To compare increases in the AQP1-mediated diffusion of different brain regions, the changes in ADC (s) of the main diffusion-enhanced brain regions were calculated relative to the average of the control group (Fig. S5A). Pairwise comparison of ADC changes showed that ADC changes in Hip_R and Tha_R were smaller compared to most of

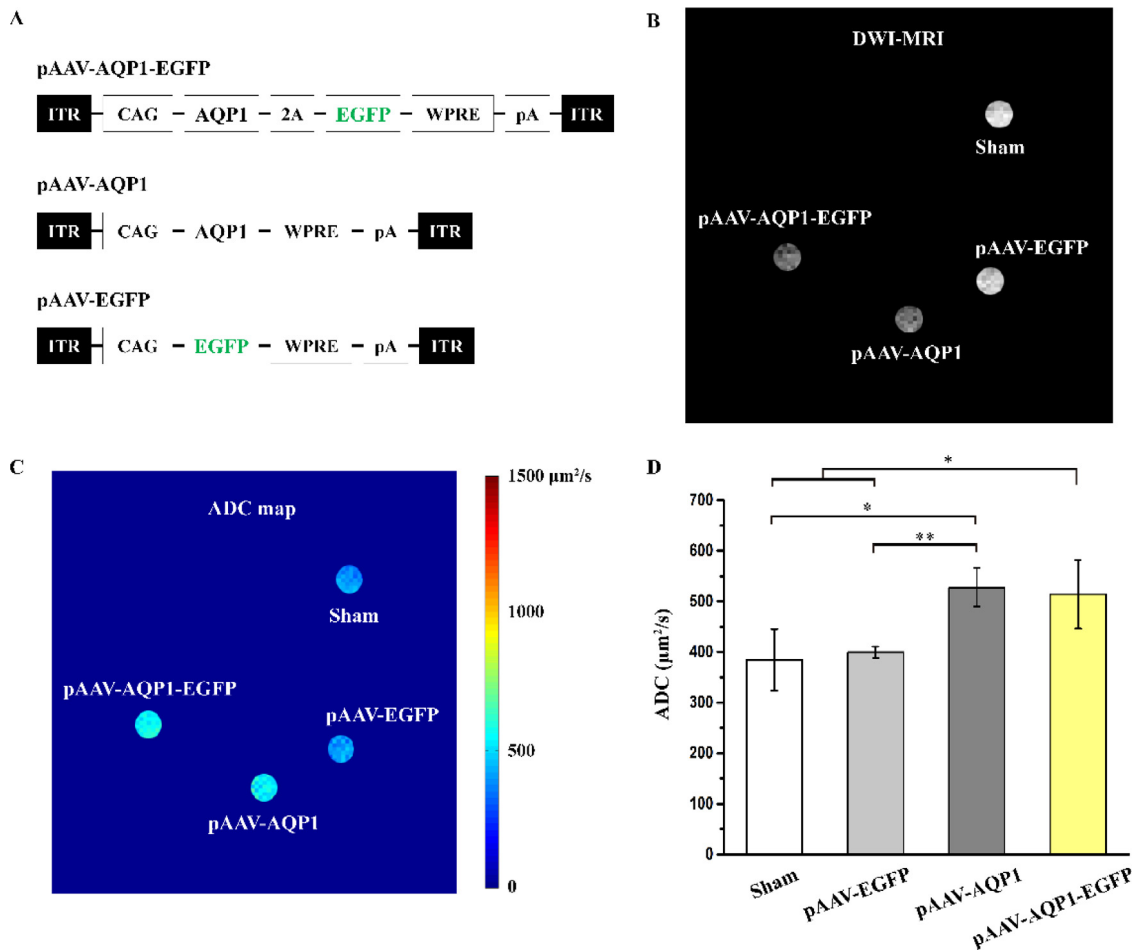


Fig. 1. Diffusion-weighted MRI (DWI-MRI) of AQP1-expressing BHK21 cells. (A) The diagram of recombinant AAV transfer plasmids encoding each gene of interest (GOI), i.e., AQP1-2A-EGFP, AQP1, or EGFP. The GOI was driven under the CAG promoter and inserted between the inverted terminal repeat sequence (ITR) to allow a ubiquitous protein expression in mammalian cells and gene packaging into the AAV particle, respectively. WPRE: Woodchuck Hepatitis Virus (WHP) Posttranscriptional Regulatory Element helped to increase transgene expression. pA: the polyA sequence. pAAV-AQP1-EGFP, pAAV-AQP1 and pAAV-EGFP represent plasmid names. (B) DWI images of cells expressing AQP1-EGFP, AQP1, or EGFP. BHK21 cells were transfected with AAV transfer plasmids and subjected to *in vitro* DWI. Sham is the untransfected cell control. (C) ADC map of cells corresponding to the DWI images. (D) Average ADC values of each group. Error bars represent the means of ADC \pm standard error of means. * $p < 0.05$; ** $p < 0.01$.

the other brain regions (Fig. S5B). These results indicate that BLA_R, Ctx_R, Ctx_L, Ins_R and Ins_L sent stronger projections to the CPU, while Hip_R and Tha_R sent moderate projections to the CPU. Our results are basically consistent with the previously reported quantitative analysis (Dudman et al., 2010; Tervo et al., 2016). Therefore, the change in ADC of a given brain region could partially reflect the strength of inputs that project from this region to the CPU. However, the rAAV-retro virus might have different infection efficacies and tropisms for different types of neurons in different brain regions, which could also affect the AQP1 expression in brain regions (Zhu et al., 2019).

4.4. Detection of cell type-specific neural connections with *in vivo* DWI

The mammalian neurons consist of diverse cell types. It is, thereby, critical to characterize the roles of specific cell types in neural networks. In this study, the cell type-specific neural connection of CPU was explored using the rAAV2-retro vector that specifically delivers transgene into the Thy1-positive neurons of the Thy1-Cre transgenic mouse ($n = 5/\text{group}$). The Cre-dependent AQP1 expression cassette was inserted into the rAAV transfer plasmid (P5) (Fig. 6A) to generate the rAAV-retro-DIO-AQP1-EGFP for injecting into the CPU of the Thy1-Cre

mouse. Three weeks after the infection, the living mouse brain was imaged using *in vivo* DWI.

The ADC maps in mice brains infected with the rAAV-retro-DIO-AQP1-EGFP and rAAV-retro-DIO-EGFP (as an AQP1 negative control) were calculated and compared. The t values of significant changes were overlapped on the homemade template as a color dimension (Fig. 6B). Several brain regions, including Ctx, CPU, Ins, Tha, and BLA of the rAAV-retro-DIO-AQP1-EGFP group, showed significantly higher ADC values than those in the rAAV-retro-DIO-EGFP. In the rAAV-retro-DIO-AQP1-EGFP group, the extensive superimpose of the hypointense DWI contrast and EGFP signals were detected in the whole brain (Fig. 6B, C). Furthermore, the EGFP-positive cells in all brain regions that showed DWI contrast were identified as Cre-positive (Thy1-positive) neurons (Fig. S6). This evidence suggests that our system could be implemented to investigate the CPU-connected upstream areas of Thy1-positive neurons.

5. Discussion

Dissection of the neural connection structures, especially in living animals, is essential to decipher their roles in information processing and guiding behavior. The current study presents an integration of two at-

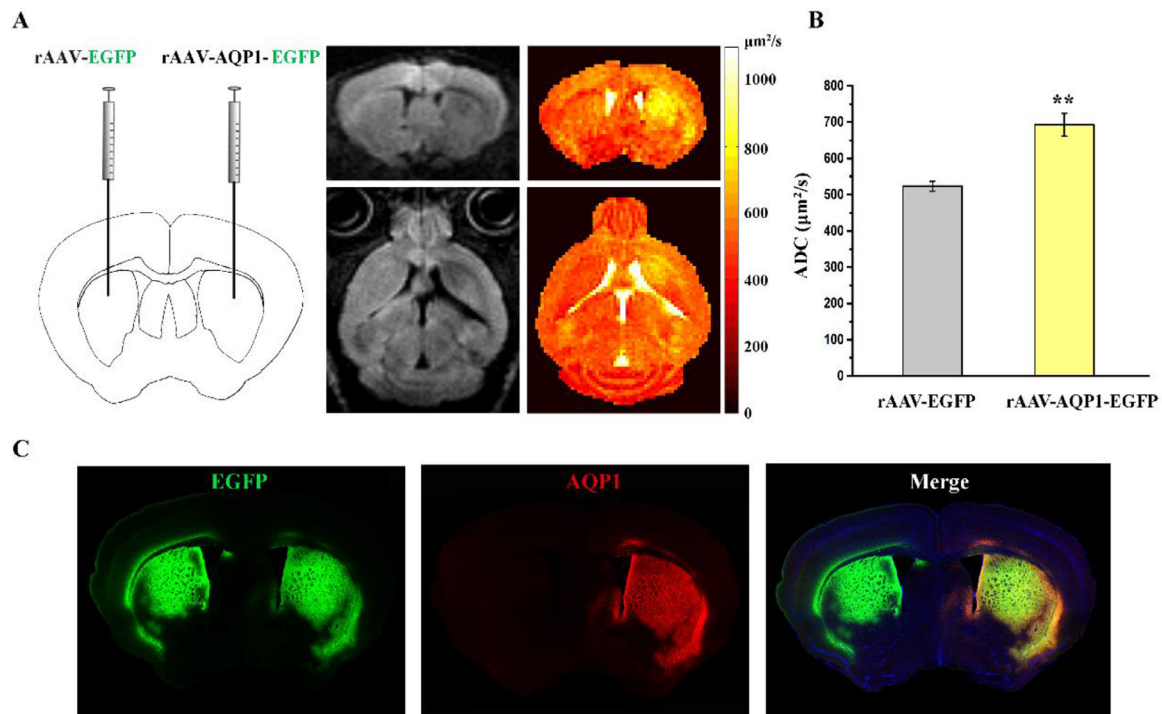


Fig. 2. Detection of AQP1 expression in the mouse brain using DWI-MRI and fluorescent imaging. (A) Representative diffusion-weighted images and ADC maps of a coronal and horizontal brain slice injected with rAAV-EGFP and rAAV-AQP1-EGFP at the bilateral CPU regions. The mouse brain was imaged by *in vivo* DWI at 21 days after injection to determine (B) average ADC values and (C) Fluorescence imaging of the bilateral CPU. DWI images of four mice were included in the ADC comparison. Error bars represent the means of the ADC \pm standard error of means. ** $p < 0.01$. The expression of AQP1 in the CPU region was detected by immunohistochemistry staining (red) signals using rabbit anti-AQP1 and a Cy3-conjugated goat anti-rabbit antibodies as primary and secondary antibodies..

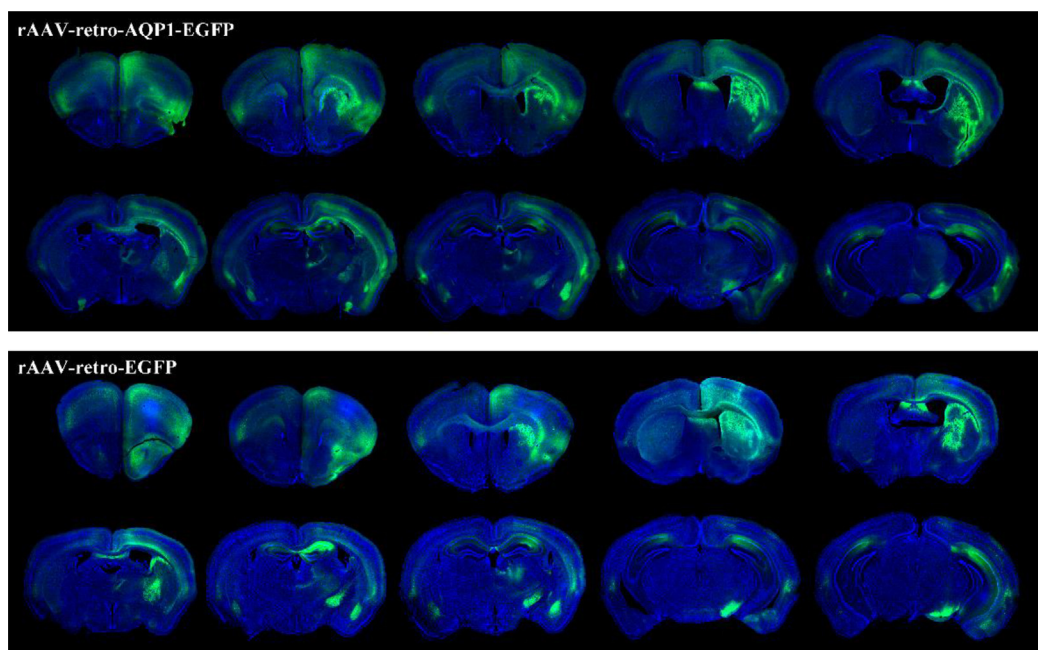


Fig. 3. The EGFP fluorescent images of mice injected with AQP1-EGFP or EGFP expressing rAAV2-retro vectors. The rAAV2-retro vectors expressing AQP1-EGFP (rAAV-retro-AQP1-EGFP) or EGFP (rAAV-retro-EGFP) were injected in CPU regions of the mouse brain. The patterns of the green fluorescent signal for rAAV-retro-AQP1-EGFP and the rAAV-retro-EGFP group are similar suggesting that these two different rAAV2-retro vectors mainly spread into the same brain regions.

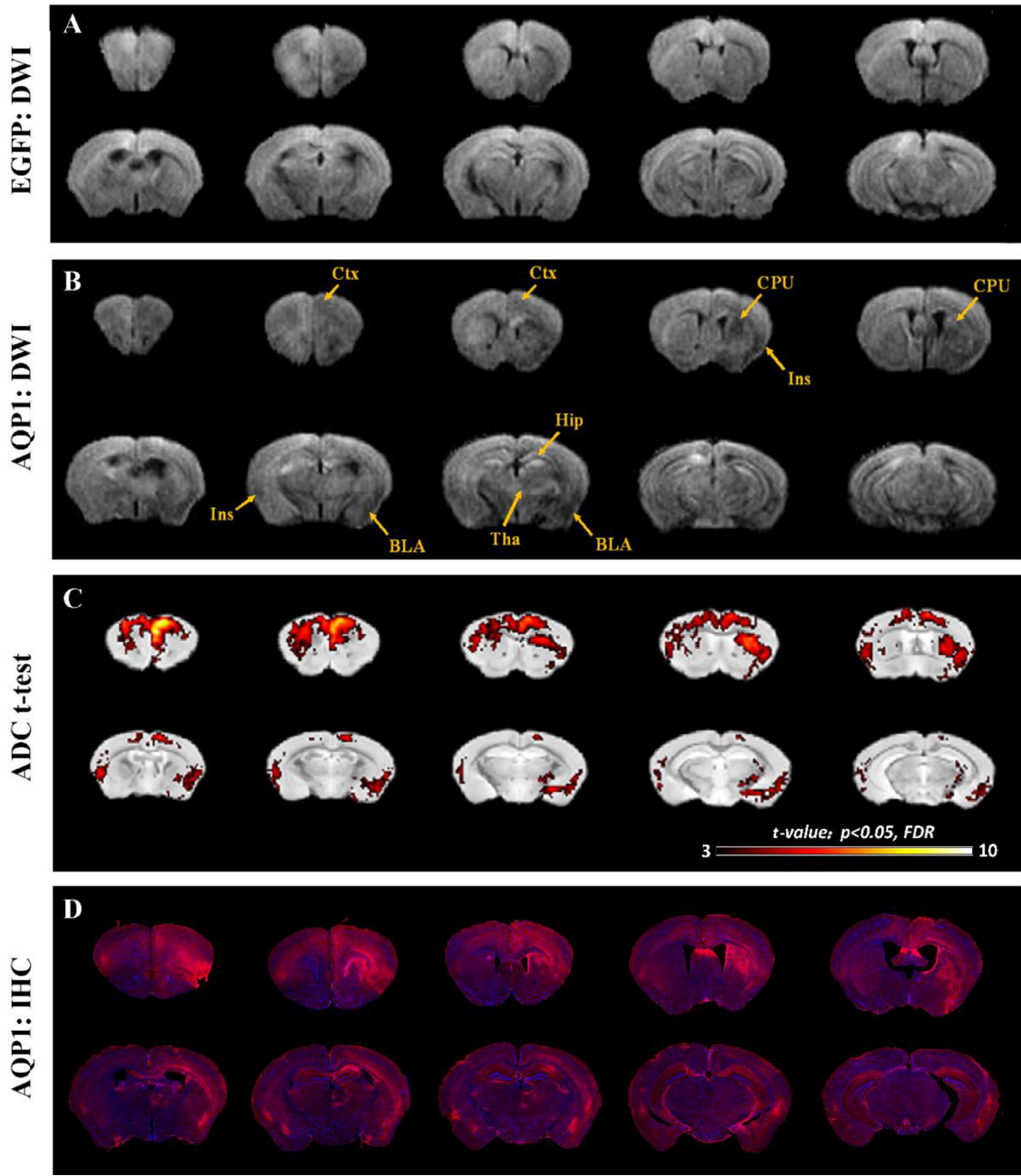


Fig. 4. DWI-MRI and immunohistochemistry staining in the CPU region of the mouse brain injected with the rAAV-retro-EGFP and rAAV-retro-AQP1-EGFP. Diffusion-weighted images of brain slices of a mouse injected with (A) rAAV-retro-EGFP and (B) rAAV-retro-AQP1-EGFP. Several brain regions showed hypointensity DWI signals, including the right CPU, Ctx, BLA, Ins, right Tha and right HIP. (C) ADC values in the brain of the rAAV-retro-AQP1-EGFP group compared to the rAAV-retro-EGFP group were calculated by the voxel-by-voxel *t*-test. The colorbar represents the *t* score obtained by the Student's *t*-test. Brighter (or whiter) color indicates a greater difference. Five mice were included in each group. (D) AQP1 immunohistochemistry staining in the rAAV-retro-AQP1-EGFP group. Red fluorescent signals represent the expression of the AQP1 protein. Cell nuclei were counterstained with DAPI (blue).

tractive techniques, the MRI reporter-encoding rAAV2-retro and *in vivo* DWI, that are beneficial for the study of brain-wide neural connection *in vivo*. AQP1-EGFP encoding rAAV2-retro was utilized to label the CPU-connected network, and *in vivo* DWI was used to visualize the labeled neural circuits. Combined with the Cre-dependent expression cassette and Cre-transgenic mouse line, the methods precisely allow the investigation of cell type-specific neural networks *in vivo*. The strategy proposed here could facilitate a longitudinal study of neural networks in rodent and possibly non-human primates.

5.1. MRI reporter genes that might be harnessed in the current neural circuit detection strategy

Unlike MEMRI or DTI, the current neural circuit detection strategy is based on the combination of neurotropic viruses and MRI reporter genes, which brings the following advantages. First, the *in vivo* brain-wide information of neural connectivity could be readily verified by the detailed structures of the reporter-labeled neural cell bodies and fibers within individuals. Second, the neural connection of a given cell-type

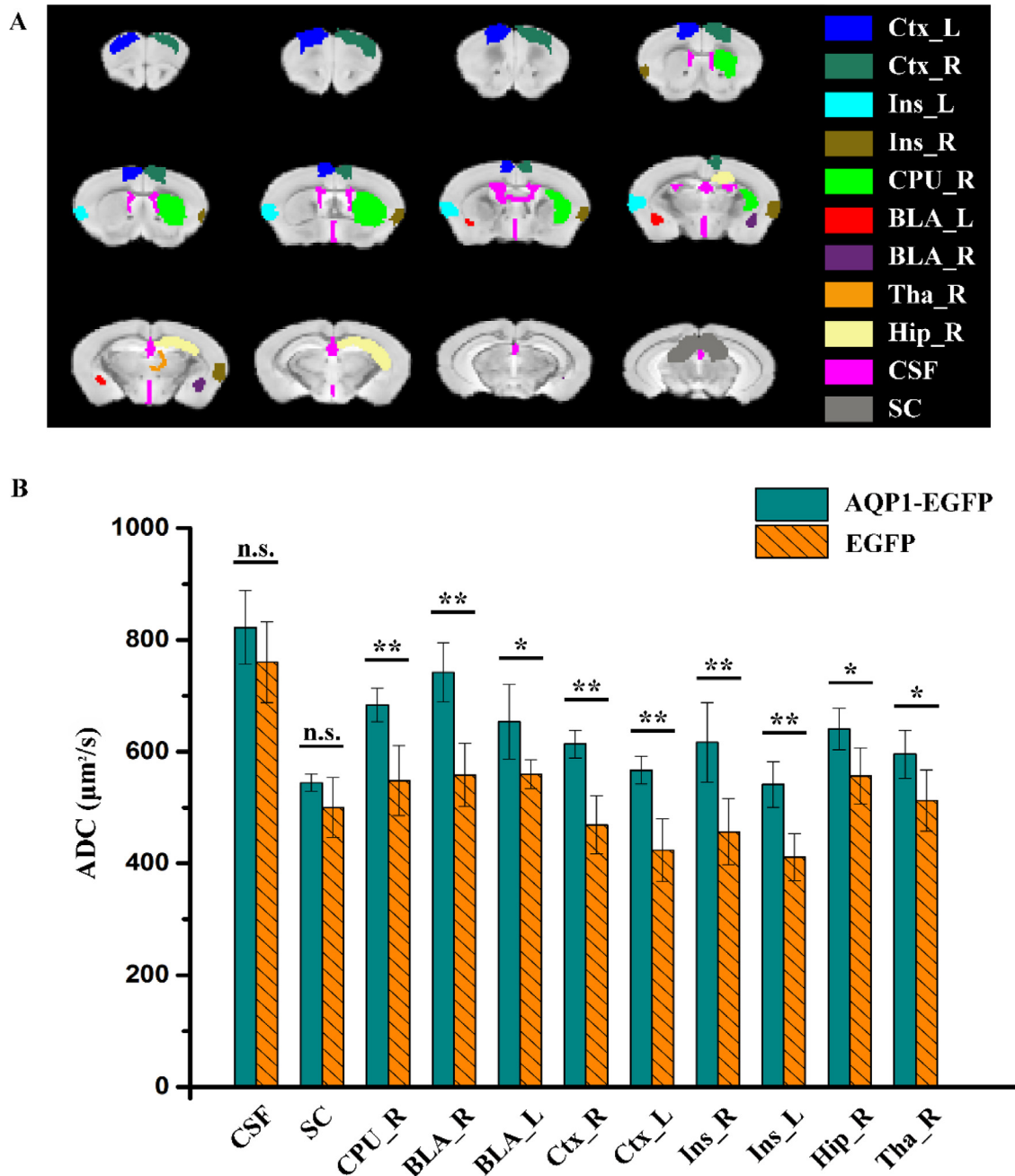


Fig. 5. Comparison of the ADC values of the AQP1 transduction areas in the mouse brains injected with rAAV-AQP1-EGFP or rAAV-EGFP at the CPU region. **(A)** The segmented selected regions (AQP1 transduction areas) of the mouse brain. Ctx: cerebral cortex, Ins: insular cortex, CPU: caudate putamen, BLA: basolateral amygdala, Tha: thalamus, HIP: hippocampus, CSF: cerebrospinal fluid, SC: superior colliculus. R: Right. L: Left. **(B)** ADC values of each region were analyzed by the *t*-test. CSF and SC were selected as negative controls. Error bars represent means of ADC values \pm standard error of means * $p < 0.05$; ** $p < 0.01$.

or a specific direction could be traced *in vivo*. The MRI reporter gene is the critical element for visualization. The characteristics of the MRI reporter, such as stabilizing in the rAAV genome, adequate expression, proper protein folding, and providing sufficient MRI contrast without exogenous reagents, are essential for distinguished visualization in the current strategy. Here, the advantages and limitations of genetically encoded MRI reporters are described regarding their biological function and sensitivity.

Ferritin is one of the most studied MRI reporter gene, and it causes strong hypointense MRI contrast through recruiting iron ions. However, this is influenced by the abundance of iron in the intracellular environment and iron ions' supplement rate, resulting in a time de-

lay between ferritin expression and MRI signal change, as reported in previous studies (Cai et al., 2021; Zheng et al., 2019). Unlike ferritin, the AQP1 alters the DWI-MRI signal by affecting the diffusion of water molecules which can lower the latency time between AQP1 expression and MRI signal change compared to the ferritin (Cai et al., 2021). The urea transporter (UT-B) alters transmembrane water exchange and was recently identified as a sensitive MRI reporter (Schilling et al., 2017). Nonetheless, the specifically designed pulse sequences are required to obtain the MRI signal through filter-exchange imaging (FEXI). The MRI contrast caused by the AQP1 could be directly detected by the stimulated-echo-based DWI pulse sequence, which is ubiquitous in a standard MRI equipment (Mukherjee et al., 2016; Schilling et al.,

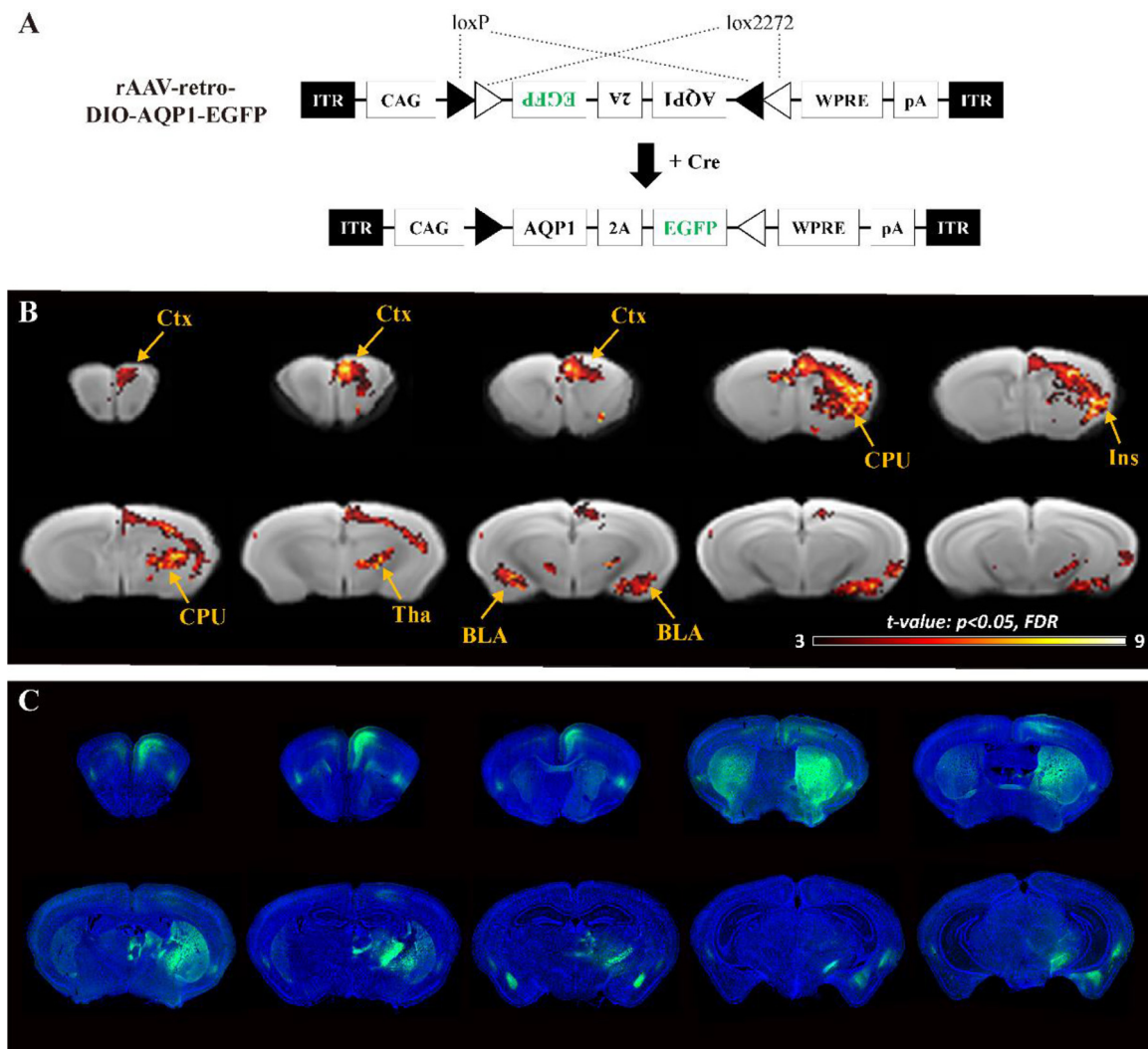


Fig. 6. DWI-MRI and fluorescent images of mice injected with rAAV-retro encoding DOI-AQP1-EGFP or DIO-EGFP. (A) The diagram of the rAAV2-retro virus genome that encoded the Cre-dependent AQP1-EGFP gene. The black and white triangles represent two different loxP sites to allow AQP1-GFP expression in the presence of Cre recombinase. AQP1-EGFP expression only occurs in cells expressing the Cre recombinase. (B) ADC values of brains of mice injected with the rAAV-DIO-AQP1-EGFP compared with the rAAV-retro-DIO-EGFP using the voxel-by-voxel *t*-test. Five mice were included in each group. (C) The EGFP fluorescence images of a mouse brain in the rAAV-retro-DIO-AQP1-EGFP group.

2017). Furthermore, the divalent metal transporter, DMT1, that allows increased manganese uptake in DMT1 expressing cells, was demonstrated as a reporter gene. It could sensitively be detected with enhanced MEMRI signal (Bartelle et al., 2013). However, the systemic exposure to manganese toxicity might limit its application and clinical translation. The organic anion transporting protein, Oatp1a1, mediates the uptake of a Gd^{3+} -based MRI contrast agent and produces intense T1-weighted MRI contrast. It also provides large positive MRI contrast with restricted background (Patrick et al., 2014). Since the Gd^{3+} -based MRI contrast agents have been approved clinically, the Oatp1a1 based MRI reporter system is promising for future clinical translation. Thus, the Oatp1a1 gene could be cloned into a rAAV genome and used to optimize the current method in the future. The artificially engineered fMRI reporter genes, nitric oxide synthases for targeting image contrast (NOSTICs), were established and validated in a recent paper (Ghosh et al., 2022). NOSTIC probes can transduce cytosolic calcium dynamics to localized hemodynamic responses through the local formation of the gaseous vasodilator nitric oxide (NO), so that they can report neural activation and allow functional dissection of the neural circuit. Although AQP1-encoding viral vectors were designed and utilized to trace the structural neural connections in the current study, the AQP1 has the

potential to be engineered as a functionally responsive reporter like NOSTIC.

5.2. rAAV vector serotypes that could be utilized for in vivo neural circuit dissection

The rAAV vector has significantly advanced our understanding of both the structure and function of neural networks (Betley and Sternson, 2011; Chan et al., 2017; Tenenbaum et al., 2004). AAVs have been classified into numerous serotypes according to their distinct capsid structures, resulting in differences in tissue tropism and transport characteristics (Agbandje-McKenna and Kleinschmidt, 2011). The rAAVs can anterograde, retrograde, or bidirectionally transport in neurons and neural circuits dependent on their serotypes and concentrations. For example, AAV1 and AAV9 serotypes are anterograde trans-synaptic viruses specifically enabling cross-synapse transduction for anterograde neural network labeling (Haggerty et al., 2020; Zingg et al., 2017). The AAV5 carrying glial fibrillary acidic protein (GFAP)/GfaABC1D promoter for astrocyte targeting (Griffin et al., 2019; Yu et al., 2020) could be used to study synaptic connections between neurons and astrocytes. The rAAV2-retro vector applied in the current study enters neurons from nerve ter-

minals, retrograde transports to the axon, and reaches the nucleus for gene transduction (Tervo et al., 2016). With the help of other kinds of AQP1 encoding rAAV vectors, the neural networks of the spread in different directions could be dissected *in vivo*.

5.3. Dissection of the cell type-specific neural circuit

The mammalian neurons include numerous cell types connected to the network via trillions of synapses. It is critical to restrict the transduction of the reporter or modulator genes in specific cell populations within precise locations of circuits of interest (Luo et al., 2008, 2018) so as to dissect the participating cell types and their connections in neural networks. Combined with a Cre/loxP-mediated recombination strategy, the insertion of the DIO element together with the gene of interest in the rAAV genome is advantageous for promoting transgene expression in the specific neuronal cell types expressing Cre recombinase (McLellan et al., 2017; Van Duyn, 2001). The rAAV vector and Cre/Loxp-based recombination were used in our study to provide transgene expression in a specific neuron type (Thy1-positive neurons). The neural connections of other neuron types could be dissected using other Cre line transgenic mice, such as DAT-Cre mice, which could be an important application to the current method. Using cell type-specific promoters is another procedure to improve transgene expression in particular cells. For instance, Ca^{2+} /calmodulin-dependent protein kinase II alpha (CamKIIa) promoter was applied to restrict the transgene expression in neurons expressing CamKIIa (Kellendonk et al., 2006; Tsien et al., 1996).

5.4. The MRI scanning time could be shortened

The DWI-MRI experiments in the current study were conducted on a 7T MRI scanner with a fifty-one-minute spin-echo-based DWI pulse sequence, which is time-consuming. In future application, the MRI scanning could be implemented on an MRI scanner of higher field strength to obtain higher sensitivity and reduce the scanning time without affecting the signal-to-noise ratio. We performed the MRI experiments on a 9.4 Tesla scanner with a thirteen-minute echo-planar imaging-based DWI sequence (EPI-DWI). The results showed that the dark DWI signals of virus-infected regions were also apparent on 9.4T MRI images (Fig. S7). Thus, the MRI scanning time in a further application study could be efficiently shortened with a higher field MRI scanner.

5.5. Limitation and perspectives

The neural circuit detection method based on the *in vivo* MRI could be beneficial for conducting longitudinal studies and translational research, and is convenient as it provides brain-wide global information for further local histology and optical studies. However, there are still some limitations to be solved in future studies. For instance, the *t*-test maps of the *in vivo* MRI results were partially overlapped with the fluorescent images, which could be caused by the following reasons. Firstly, the fluorescent images are the representative images from an individual mouse, while the *t*-test maps were the results of group analysis. Secondly, the slice thickness was different (800 μ m vs 40 μ m), and the angle of the imaging was very difficult to be kept exactly the same. Thirdly, the fixation and frozen section of the tissue for optical imaging could cause the shrinkage or other distortions to the slices. In addition, the relatively low spatial resolution of the MRI makes it difficult to distinguish small brain regions or sub-regions. Another limitation is the relatively low MRI SNR (signal-to-noise ratio) of the DWI sequences. At first, the *b* value was set to 1000 s/mm² in the diffusion weighted imaging, which attenuated the MRI signals. Then, we accessed long diffusion times (100 ms) by stimulated echo DWI according to a previous reported study (Mukherjee et al., 2016). The stimulated echo here was produced by three 90° pulses. The stimulated echo intensity is only half of a spin echo taken at the same readout time (i.e., the time corresponding to the first and third intervals of the three-pulse sequence). The higher field

strength of the MRI scanner and longer imaging time can, to some extent, alleviate this problem.

To target a specific brain region, the rAAV vectors were stereotactically injected into the brain regions in this study, which is slightly invasive. Through a completely non-invasive technology, the focused ultrasound blood-brain barrier opening (FUS-BBBO), rAAV could also be directly delivered to the targeted brain region. The FUS-BBBO has been verified to permit the delivery of multiple AAV serotypes to the brain in several animal species (Alonso et al., 2013; Choi et al., 2007; Szabowski et al., 2018; Thévenot et al., 2012; Wang et al., 2015). Combining the non-invasive gene delivery and MRI imaging, this *in vivo* neural connection tracing strategy could open a new avenue for neural circuit study in non-human primates (Carpentier et al., 2016). Furthermore, the AQP1-encoding rAAV vector would simultaneously deliver functional elements such as channelrhodopsin-2 (ChR2) and human M3 muscarinic DREADD (hM3Dq) to investigate neuronal functions using optogenetic and chemogenetic techniques, respectively. Together with the *in vivo* MRI, these approaches could also be beneficial for further neural manipulation.

6. Conclusion

The current work proposed a novel approach that enables *in vivo* detection of brain-wide neural connections. With the insertion of the AQP1 gene in the rAAV2-retro and DWI-MRI imaging method, the CPU-connected upstream network was dissected *in vivo*. The CPU-connected cell type-specific network was also successfully examined with the *in vivo* DWI-MRI in a Cre-transgenic mouse line transduced by the rAAV2-retro encoding Cre-dependent AQP1 gene. These strategies are valuable for longitudinal studies examining dynamic changes in neural networks under physiological and pathological conditions. They would facilitate the neural-network analysis in larger animals such as non-human primates.

Funding

We acknowledge the financial support by the National Natural Science Foundation of China (31970973, 31771193, 21921004), the National Key Research and the Development Program of China (2021M693294), the Key-Area Research and Development Program of Guangdong Province (2018B030331001), the Strategic Priority Research Program of the Chinese Academy of Sciences (XDB32030200), the Shenzhen Key Laboratory of Viral Vectors for Biomedicine (ZDSYS20200811142401005), the National Natural Science Foundation (NSF) of Hubei Province (2020CFA059), the Open Project Program of Wuhan National Laboratory for Optoelectronics (2019WNLOKF022).

Declaration of Competing Interest

The authors declare no competing interests.

Credit authorship contribution statement

Ning Zheng: Visualization, Formal analysis, Investigation, Writing – original draft. **Mei Li:** Visualization, Formal analysis, Investigation, Writing – original draft. **Yang Wu:** Visualization, Formal analysis, Investigation. **Challika Kaewborisuth:** Writing – review & editing. **Zhen Li:** Investigation. **Zhu Gui:** Formal analysis. **Jinfeng Wu:** Formal analysis. **Aoling Cai:** Formal analysis. **Kangguang Lin:** Visualization, Formal analysis, Investigation. **Kuan-Pin Su:** Writing – review & editing. **Hongbing Xiang:** Visualization, Formal analysis, Investigation. **Xuebi Tian:** Visualization, Formal analysis, Investigation. **Anne Manyande:** Writing – review & editing. **Fuqiang Xu:** Visualization, Formal analysis, Investigation. **Jie Wang:** Supervision, Writing – review & editing.

Acknowledgments

The authors would like to express their gratitude to Ms. Qitian Wang, and Ms. Dingyu Jin for technical support.

Supplementary materials

Supplementary material associated with this article can be found, in the online version, at doi:10.1016/j.neuroimage.2022.119402.

References

- Agbandje-McKenna, M., Kleinschmidt, J., 2011. AAV capsid structure and cell interactions. In: Snyder, R.O., Moullier, P. (Eds.), *Adeno-Associated Virus: Methods and Protocols*. Humana Press, Totowa, NJ, pp. 47–92.
- Alonso, A., Rein, E., Leuchs, B., Kleinschmidt, J., Fatar, M., Geers, B., Lentacker, I., Hennerici, M.G., de Smedt, S.C., Meairs, S., 2013. Focal delivery of AAV2/1-transgenes into the rat brain by localized ultrasound-induced BBB opening. *Mol. Ther. Nucl. Acids* 2, e73.
- Bartelle, B.B., Szulc, K.U., Suero-Abreu, G.A., Rodriguez, J.J., Turnbull, D.H., 2013. Divalent metal transporter, DMT1: a novel MRI reporter protein. *Magn. Reson. Med.* 70, 842–850.
- Betley, J.N., Sternson, S.M., 2011. Adeno-associated viral vectors for mapping, monitoring, and manipulating neural circuits. *Hum. Gene Ther.* 22, 669–677.
- Cai, A., Zheng, N., Thompson, G.J., Wu, Y., Nie, B., Lin, K., Su, P., Wu, J., Manyande, A., Zhu, L., Wang, J., Xu, F., 2021. Longitudinal neural connection detection using a ferritin-encoding adeno-associated virus vector and *in vivo* MRI method. *Hum. Brain Mapp.* 42, 5010–5022.
- Callaway, E.M., 2008. Transneuronal circuit tracing with neurotropic viruses. *Curr. Opin. Neurobiol.* 18, 617–623.
- Carpentier, A., Canney, M., Vignot, A., Reina, V., Beccaria, K., Horodyckid, C., Karachi, C., Leclercq, D., Lafon, C., Chapelon, J.Y., Capelle, L., Cornu, P., Sanson, M., Hoang-Xuan, K., Delattre, J.Y., Idhah, A., 2016. Clinical trial of blood-brain barrier disruption by pulsed ultrasound. *Sci. Transl. Med.* 8 343re342–343re342.
- Chan, K.Y., Jang, M.J., Yoo, B.B., Greenbaum, A., Ravi, N., Wu, W.L., Sanchez-Guardado, L., Lois, C., Mazmanian, S.K., Deverman, B.E., Gradinaru, V., 2017. Engineered AAVs for efficient noninvasive gene delivery to the central and peripheral nervous systems. *Nat. Neurosci.* 20, 1172–1179.
- Choi, J.J., Pernot, M., Small, S.A., Konofagou, E.E., 2007. Noninvasive, transcranial and localized opening of the blood-brain barrier using focused ultrasound in mice. *Ultrasound Med. Biol.* 33, 95–104.
- Cohen, B., Dafni, H., Meir, G., Harmelin, A., Neeman, M., 2005. Ferritin as an endogenous MRI reporter for noninvasive imaging of gene expression in C6 glioma tumors. *Neoplasia* 7, 109–117.
- Davidson, B.L., Breakefield, X.O., 2003. Viral vectors for gene delivery to the nervous system. *Nat. Rev. Neurosci.* 4, 353–364.
- Davidson, M., Wang, G., Aldrin-Kirk, P., Cardoso, T., Nolbrant, S., Hartnor, M., Mudanayake, J., Parmar, M., Björklund, T., 2019. A systematic capsid evolution approach performed *in vivo* for the design of AAV vectors with tailored properties and tropism. *Proc. Natl. Acad. Sci.* 116, 27053–27062.
- Donahue, C.J., Sotiropoulos, S.N., Jbabdi, S., Hernandez-Fernandez, M., Behrens, T.E., Dyrby, T.B., Coalson, T., Kennedy, H., Knoblauch, K., Van Essen, D.C., Glasser, M.F., 2016. Using diffusion tractography to predict cortical connection strength and distance: a quantitative comparison with tracers in the monkey. *J. Neurosci.* 36, 6758–6770.
- Dudman, J.T., Mao, T., Pan, W.X., 2010. Inputs to the dorsal striatum of the mouse reflect the parallel circuit architecture of the forebrain. *Front. Neuroanat.* 4.
- Dumoulin, S.O., Fracasso, A., van der Zwaag, W., Siero, J.C.W., Petridou, N., 2018. Ultra-high field MRI: advancing systems neuroscience towards mesoscopic human brain function. *Neuroimage* 168, 345–357.
- Enquist, L., 2003. Recent advances in the use of neurotropic viruses for circuit analysis. *Curr. Opin. Neurobiol.* 13, 603–606.
- Farhadi, A., Sigmund, F., Westmeyer, G.G., Shapiro, M.G., 2021. Genetically encodable materials for non-invasive biological imaging. *Nat. Mater.* 20, 585–592.
- García-Otín, A.L., 2006. Mammalian genome targeting using site-specific recombinases. *Front. Biosci.* 11, 1108.
- Genove, G., DeMarco, U., Xu, H., Goins, W.F., Ahrens, E.T., 2005. A new transgene reporter for *in vivo* magnetic resonance imaging. *Nat. Med.* 11, 450–454.
- Ghosh, S., Li, N., Schwalm, M., Bartelle, B.B., Xie, T., Daher, J.I., Singh, U.D., Xie, K., DiNapoli, N., Evans, N.B., Chung, K., Jasanoff, A., 2022. Functional dissection of neural circuitry using a genetic reporter for fMRI. *Nat. Neurosci.* 25, 390–398.
- Gilad, A.A., Winnard, P.T., van Zijl, P.C., Bulte, J.W., 2007. Developing MR reporter genes: promises and pitfalls. *NMR Biomed.* 20, 275–290.
- Gilad, A.A., Ziv, K., McMahon, M.T., van Zijl, P.C., Neeman, M., Bulte, J.W., 2008. MRI reporter genes. *J. Nucl. Med.* 49, 1905–1908.
- Griffin, J.M., Fackelmeier, B., Fong, D.M., Mouravlev, A., Young, D., O'Carroll, S.J., 2019. Astrocyte-selective AAV gene therapy through the endogenous GFAP promoter results in robust transduction in the rat spinal cord following injury. *Gene Ther.* 26, 198–210.
- Haggerty, D.L., Grecco, G.G., Reeves, K.C., Atwood, B., 2020. Adeno-associated viral vectors in neuroscience research. *Mol. Ther. Methods Clin. Dev.* 17, 69–82.
- Hoehn, M., Aswendt, M., 2013. Structure-function relationship of cerebral networks in experimental neuroscience: contribution of magnetic resonance imaging. *Exp. Neurol.* 242, 65–73.
- Huang, Z.J., 2014. Toward a genetic dissection of cortical circuits in the mouse. *Neuron* 83, 1284–1302.
- Iordanova, B., Ahrens, E.T., 2012. *In vivo* magnetic resonance imaging of ferritin-based reporter visualizes native neuroblast migration. *Neuroimage* 59, 1004–1012.
- Kellendonk, C., Simpson, E.H., Polan, H.J., Malleret, G., Vronskaya, S., Winiger, V., Moore, H., Kandel, E.R., 2006. Transient and selective overexpression of dopamine D2 receptors in the striatum causes persistent abnormalities in prefrontal cortex functioning. *Neuron* 49, 603–615.
- Le Bihan, D., 2003. Looking into the functional architecture of the brain with diffusion MRI. *Nat. Rev. Neurosci.* 4, 469–480.
- Lin, T.H., Chiang, C.W., Trinkaus, K., Spees, W.M., Sun, P., Song, S.K., 2014. Manganese-enhanced MRI (MEMRI) via topical loading of Mn(2+) significantly impairs mouse visual acuity: a comparison with intravitreal injection. *NMR Biomed.* 27, 390–398.
- Luo, L., Callaway, E.M., Svoboda, K., 2008. Genetic dissection of neural circuits. *Neuron* 57, 634–660.
- Luo, L., Callaway, E.M., Svoboda, K., 2018. Genetic dissection of neural circuits: a decade of progress. *Neuron* 98, 256–281.
- Matsumoto, Y., Jasanoff, A., 2013. Metalloprotein-based MRI probes. *FEBS Lett.* 587, 1021–1029.
- McLellan, M.A., Rosenthal, N.A., Pinto, A.R., 2017. Cre-loxP-mediated recombination: general principles and experimental considerations. *Curr. Protoc. Mouse Biol.* 7, 1–12.
- Mori, S., van Zijl, P.C., 2002. Fiber tracking: principles and strategies - a technical review. *NMR Biomed.* 15, 468–480.
- Mori, S., Zhang, J., 2006. Principles of diffusion tensor imaging and its applications to basic neuroscience research. *Neuron* 51, 527–539.
- Mukherjee, A., Davis, H.C., Ramesh, P., Lu, G.J., Shapiro, M.G., 2017. Biomolecular MRI reporters: evolution of new mechanisms. *Prog. Nucl. Magn. Reson. Spectrosc.* 102–103, 32–42.
- Mukherjee, A., Wu, D., Davis, H.C., Shapiro, M.G., 2016. Non-invasive imaging using reporter genes altering cellular water permeability. *Nat. Commun.* 7, 13891.
- Nassi, J.J., Cepko, C.L., Born, R.T., Beier, K.T., 2015. Neuroanatomy goes viral! *Front. Neuroanat.* 9, 80.
- Park, H.J., Friston, K., 2013. Structural and functional brain networks: from connections to cognition. *Science* 342, 1238411.
- Patrick, P.S., Hammersley, J., Loizou, L., Kettunen, M.L., Rodrigues, T.B., Hu, D.E., Tee, S.S., Heske, R., Lyons, S.K., Soloviev, D., Lewis, D.Y., Aime, S., Fulton, S.M., Brindle, K.M., 2014. Dual-modality gene reporter for *in vivo* imaging. *Proc. Natl. Acad. Sci.* 111, 415–420.
- Pautler, R.G., Silva, A.C., Koretsky, A.P., 1998. *In vivo* neuronal tract tracing using manganese-enhanced magnetic resonance imaging. *Magn. Reson. Med.* 40, 740–748.
- Pfister, H., Kaynig, V., Botha, C., Bruckner, S., Derksen, V., Hege, H.C., Roerdink, J., 2012. Visualization in connectomics. *Math. Vis.* 37, 221–245.
- Roselli, F., Caroni, P., 2012. A circuit mechanism for neurodegeneration. *Cell* 151, 250–252.
- Rubinov, M., Bullmore, E., 2013. Fledgling pathoconnectomics of psychiatric disorders. *Trends Cogn. Sci.* 17, 641–647.
- Saar, G., Koretsky, A.P., 2019. Manganese enhanced MRI for Use in studying neurodegenerative diseases. *Front. Neural Circuits* 12, 114.
- Schilling, F., Ros, S., Hu, D.E., D'Santos, P., McGuire, S., Mair, R., Wright, A.J., Mannion, E., Franklin, R.J.M., Neves, A.A., Brindle, K.M., 2017. MRI measurements of reporter-mediated increases in transmembrane water exchange enable detection of a gene reporter. *Nat. Biotechnol.* 35, 75–80.
- Shenton, M.E., Dickey, C.C., Frumin, M., McCarley, R.W., 2001. A review of MRI findings in schizophrenia. *Schizophr. Res.* 49, 1–52.
- Szabolowski, J.O., Lee-Gosselin, A., Lue, B., Malounda, D., Shapiro, M.G., 2018. Acoustically targeted chemogenetics for the non-invasive control of neural circuits. *Nat. Biomed. Eng.* 2, 475–484.
- Tenenbaum, L., Chharta, A., Lehtonen, E., Velu, T., Brothi, J., Levivier, M., 2004. Recombinant AAV-mediated gene delivery to the central nervous system. *J. Gene Med.* 6, S212–S222.
- Tervo, D.G., Hwang, B.Y., Viswanathan, S., Gaj, T., Lavzin, M., Ritola, K.D., Lindo, S., Michael, S., Kuleshova, E., Ojala, D., Huang, C.C., Gerfen, C.R., Schiller, J., Dudman, J.T., Hantman, A.W., Looger, L.L., Schaffer, D.V., Karpova, A.Y., 2016. A designer AAV variant permits efficient retrograde access to projection neurons. *Neuron* 92, 372–382.
- Thévenot, E., Jordão, J.F., O'Reilly, M.A., Markham, K., Weng, Y.Q., Foust, K.D., Kaspar, B.K., Hynynen, K., Aubert, I., 2012. Targeted delivery of self-complementary adeno-associated virus serotype 9 to the brain, using magnetic resonance imaging-guided focused ultrasound. *Hum. Gene Ther.* 23, 1144–1155.
- Tsien, J.Z., Chen, D.F., Gerber, D., Tom, C., Mercer, E.H., Anderson, D.J., Mayford, M., Kandel, E.R., Tonegawa, S., 1996. Subregion- and cell type-restricted gene knockout in mouse brain. *Cell* 87, 1317–1326.
- Ugolini, G., 2010. Advances in viral transneuronal tracing. *J. Neurosci. Methods* 194, 2–20.
- Van Duyn, G.D., 2001. A structural view of Cre-loxP site-specific recombination. *Annu. Rev. Biophys. Biomol. Struct.* 30, 87–104.
- Wang, S., Olumolade, O.O., Sun, T., Samiotaki, G., Konofagou, E.E., 2015. Noninvasive, neuron-specific gene therapy can be facilitated by focused ultrasound and recombinant adeno-associated virus. *Gene Ther.* 22, 104–110.
- Wu, Y., Han, Z., Duan, M., Jiang, L., Tian, T., Jin, D., Wang, Q., Xu, F., 2021. Popularizing recombinant baculovirus-derived onebac system for laboratory production of all recombinant adeno-associated virus vector serotypes. *Curr. Gene Ther.* 21, 167–176.
- Wu, Y., Jiang, L., Geng, H., Yang, T., Han, Z., He, X., Lin, K., Xu, F., 2018. A recombinant baculovirus efficiently generates recombinant adeno-associated virus vectors in cultured insect cells and larvae. *Mol. Ther. Methods Clin. Dev.* 10, 38–47.

- Yi-Jen Lin, A.P.K., 1997. Manganese ion enhances T1-weighted MRI during brain activation: an approach to direct imaging of brain function. *Magn. Reson. Med.* 38, 378–388.
- Yu, X., Nagai, J., Khakh, B.S., 2020. Improved tools to study astrocytes. *Nat. Rev. Neurosci.* 21, 121–138.
- Zheng, N., Su, P., Liu, Y., Wang, H.D., Nie, B.B., Fang, X.H., Xu, Y., Lin, K.Z., Lv, P., He, X.B., Guo, Y., Shan, B., Manyande, A., Wang, J., Xu, F.Q., 2019. Detection of neural connections with ex vivo MRI using a ferritin-encoding trans-synaptic virus. *Neuroimage* 197, 133–142.
- Zheng, N., Wang, Z.Z., Wang, S.W., Yang, F.J., Zhu, X.T., Lu, C., Manyande, A., Rao, X.P., Xu, F.Q., 2020. Co-localization of two-color rAAV2-retro confirms the dispersion characteristics of efferent projections of mitral cells in mouse accessory olfactory bulb. *Zool. Res.* 41, 148–156.
- Zhu, X., Lin, K., Liu, Q., Yue, X., Mi, H., Huang, X., He, X., Wu, R., Zheng, D., Wei, D., Jia, L., Wang, W., Manyande, A., Wang, J., Zhang, Z., Xu, F., 2019. Rabies virus pseudotyped with CVS-N2C glycoprotein as a powerful tool for retrograde neuronal network tracing. *Neurosci. Bull.* 36, 202–216.
- Zingg, B., Chou, X.L., Zhang, Z.G., Mesik, L., Liang, F., Tao, H.W., Zhang, L.L., 2017. AAV-mediated anterograde transsynaptic tagging: mapping corticocollicular input-defined neural pathways for defense behaviors. *Neuron* 93, 33–47.